Hindawi
Nanomaterials and Nanotechnology
Volume 2023, Article ID 3603680, 14 pages
https://doi.org/10.1155/2023/3603680

Research Article

Rapid Colorimetric Detection of Hg (II) Based on Hg (II)-Induced Suppressed Enzyme-Like Reduction of 4-Nitrophenol by Au@ ZnO/Fe_3O_4 in a Cosmetic Skin Product

Oratile Semong and Bareki Shima Batlokwa

Department of Chemical and Forensic Sciences, College of Science, Botswana International University of Science and Technology, Plot 10071, Private Bag 16, Palapye, Botswana

Correspondence should be addressed to Oratile Semong; mogapaesio@biust.ac.bw

Received 27 June 2023; Revised 30 October 2023; Accepted 1 November 2023; Published 11 November 2023

Academic Editor: Nico Lovergine

Herein, we synthesized gold-coated ZnO/Fe_3O_4 nanocomposites. Initially, we prepared Fe_3O_4 magnetic nanoparticles based on the co-precipitation of Fe^{3+} and Fe^{2+} under aqueous ammonia as a precipitating agent. Thereafter, the ZnO/Fe_3O_4 composite was prepared by dispersing the synthesized magnetic nanoparticles into an alkaline zinc nitrate solution. After calcination of the precipitate, the formed ZnO/Fe_3O_4 composites were coated with gold nanostructures by dispersing the composites in auric acid/ethylene glycol solution in a water bath. The synthesized $Au@ZnO/Fe_3O_4$ hybrid material was able to catalyze the reduction of 4-nitrophenol (4-NP) to 4-aminophenol (4-AP). We demonstrate that this catalytic activity can be exploited for the detection of Hg^{2+} ions in a cosmetic product. In the presence of Hg^{2+} ions, the catalytic activity of $Au@ZnO/Fe_3O_4$ was greatly suppressed. This novel finding underlies a straightforward, sensitive, and highly selective detection probe for Hg^{2+}. The material exhibited excellent analytical performance as marked by the very low limit of detection (LOD) of 2.34 nM, which was well below acceptable levels of 4.99 μM for mercury in cosmetics as set by the US Food and Drug Administration (FDA), and within the linear dynamic ranges of 0–10 nM. High recoveries ranging from 96.5 to 100.3% accompanied by excellent selectivities toward Hg^{2+} over potentially interfering species were obtained.

1. Introduction

The intentional adulteration of skin-lightening cosmetics with mercury is not only fraudulent but also dangerous. Long-term use of such skin-lightening cosmetics results in respiratory, cardiovascular, gastrointestinal, hepatic, renal impairment, and reproductive effects. Moreover, mercury is associated with elevated white blood cell count, changes in autoimmune response, drop in vision, and genotoxic effects [1]. The world's leading health regulatory institutions restrict the use of mercury in cosmetics. The EU Cosmetics Regulation (EC) 1223/2009 prohibits mercury-containing cosmetic products in the EU market except for the use of thiomersal in eye products where a maximum concentration of 0.007% of mercury is permitted in eye makeup, mascara, and cleansing products [2]. The US Food and Drug Administration (FDA) under title 21 CFR 700.13 limits the amount of mercury in cosmetic products to a trace amount unavoidable under good manufacturing practice, that is, 1 ppm, except in those products intended for use around the eye, which it limits to 65 ppm [3]. Despite this, consumers continue to have access to mercury-based cosmetic products and sporadic cases as well as outbreaks of mercury poisoning still occur [4]. To ensure that these restrictions are adhered to, it is necessary to employ highly sensitive and reliable analytical methods for mercury detection.

Currently, numerous approaches based on electrochemical and optical sensors [5–7], organic chromophores or fluorophores [8–13], conjugated polymers [14], oligonucleotides [15–17], DNAase [18, 19], and proteins [20–22] have been established for the detection of Hg^{2+} ions. Unfortunately, most of these methods have the disadvantages of

low selectivity, low sensitivity, and complex synthetic process [23]. Furthermore, sophisticated instrumentation including, atomic emission spectrometry (AES), atomic absorption spectrometry (AAS), and inductively coupled plasma mass spectrometry (ICP-MS) are being used for the detection of Hg^{2+} [24, 25]. Although these methods have the advantages of high accuracy and sensitivity, they are limited to expensive sophisticated instruments that require trained professional technicians and long operation times which limit their wide use in ordinary institutions and routine detection [26]. Therefore, there is an urgent need to establish a simple, fast, cheap, and sensitive methods for the detection of Hg^{2+}.

As a convenient detection method for Hg^{2+}, colorimetric strategies have received great attention due to the advantages of easy operation, rapid visual detection, and signal visibility without the aid of any advanced instrument, and they are applicable for onsite and high throughput analysis [27]. Colorimetric-sensing tools for Hg^{2+} based on the aggregation or antiaggregation of noble metal nanoparticles have been developed [22, 28–30]. However, most of these assays are insensitive. Recently, various colorimetric methods based on enzymatic catalysis for the detection of Hg^{2+} ions have been proposed successfully due to their exclusive properties, such as simplicity, high specificity, ultrasensitivity, and naked eye detection [26]. Unfortunately, natural enzymes are easily affected by environmental factors; they are easily denatured, expensive, and time-consuming to prepare [31].

To avoid these disadvantages of natural enzymes, nanoenzymes; nanomaterials with intrinsic enzyme-like characteristics and with high catalytic efficiency and operational stability have been used for the detection of Hg^{2+} ions successfully [23, 24, 26, 31–42]. Compared with natural enzymes, nanoenzymes are more stable, easy to prepare, have high yield, low cost, and tunable structure and catalytic activity [43]. Nanozymes can catalyze various types of reactions including reduction reactions, oxidation reactions, and polymerization reactions. For example, modified metal nanoparticles can catalyze the reduction of methyl orange (MO), methyl blue (MB), and 4-nitrophenol (4-NP), the oxidation of 2,2′-azino-bis(3-ethylbenzothiazoline-6-sulfonic acid) diammonium salt (ABTS) and 3,3,5,5-tetramethylbenzidine (TMB), and the polymerization of alkyl silanes [44]. It has been reported that mercury can enhance or inhibit the enzyme-like activity of noble metal nanoparticles (NPs) which enables a label-free colorimetric assay for Hg [45–48]. In this regard, many materials based on the mercury-enhanced/suppressed mimetic activity of noble NPs have been prepared. Although these materials can selectively and sensitively detect Hg, they possess several drawbacks including deactivation caused by the aggregations due to high surface energy and van der Waals forces and poor recovery and reusability [27].

To overcome such challenges, hybrid nanoenzymes (those formed from the combination of two or more different materials) have been developed. The individual components bring distinct properties and the combined properties of the hybrid material may offer new or enhanced properties, which afford versatility in the design and tailoring of multifunctional devices [49]. Among the plethora of possible components of such hybrids, gold nanoparticles (AuNPs) in particular have attracted considerable interest in the detection of Hg^{2+} where one or more of their quantum size effects, high surface energies, and high surface-to-volume ratios can be advantageously exploited [50]. The properties of AuNPs can be readily modified because they depend on the AuNP size and shape as well as on the stabilizing ligands present on the surfaces, and all of these can be systematically modified. AuNPs possess good stability, they can be synthesized from a variety of well-established procedures, and they display a rich surface functionalization chemistry with a broad variety of organic matrices and coatings (organic compound/AuNP hybrids) and flexibility that has been exploited in the drive to afford novel hybrid multifunctional materials [51, 52]. ZnO has drawn significant research attention for decades due to its earth abundance, environmental friendliness, and excellent structural, electrical, and optical properties [53]. However, its applicability as a catalyst is limited due to the rapid recombination of electron-hole pairs caused by its wide and direct bandwidth [54]. Thus, its catalytic performance can be improved by exploiting the surface plasmon resonance (SPR) effect of AuNPs, coupled with their strong scattering and absorption of incident light [55, 56]. Au nanostructures can produce electrons induced by the surface plasmon resonance (SPR) and inject them into the conduction band of contiguous ZnO nanostructures, thus improving their catalytic activity [57]. The magnetic property of the hybrid structure afforded by the Fe_3O_4 allows a straightforward and effective collection of the reaction mixture with an external magnet [58]. To the best of our knowledge, there are only two reports of the fabrication of Au@ZnO/Fe_3O_4 hybrid material in literature [54, 59]. In one instance, Quang and Vu [59] prepared Au/ZnO/Fe_3O_4 composites by a mixing method using polyvinyl alcohol (PVA) as a binder and in another Cervantes-Macıas et al. [54] doped AuNPs onto ZnO–Fe_3O_4 NPs by adding $HAuCl_4$ into a suspension of ZnO–Fe_3O_4, using sodium citrate as a reducing agent. These were applied in the photodegradation of tartrazine and oxidation of thioanisole, respectively.

Hence, in this work, we successfully employed, for the first time, polyol synthesis to coat ZnO/Fe_3O_4 with AuNPs. In addition, the synthesized Au@ZnO/Fe_3O_4 hybrid material exhibited the ability to catalyze the reduction of 4-nitrophenol (4-NP) to 4-aminophenol (4-AP). Interestingly, we found that the catalytic activity of Au@ZnO/Fe_3O_4 for this reaction can be significantly inhibited by Hg^{2+}. When Hg^{2+} is added to the reduction reaction system, the catalytic activity of AuNPs decreases because of the inhibition of the formation of gold-hydride species, leading to a long reaction time from 4-NP to 4-AP. We take advantage of this property to develop a novel probe for the rapid, selective, and sensitive colorimetric detection trace levels of Hg^{2+} in a skin-lightening cosmetic product.

2. Materials and Methods

2.1. Chemicals. Iron (II) sulphate heptahydrate ($FeSO_4.7H_2O$), iron (III) chloride hexahydrate ($FeCl_3.6H_2O$), zinc nitrate ($Zn(NO_3)_2$), auric acid ($HAuCl_4$), ethylene glycol (EG), sodium borohydride ($NaBH_4$), mercury nitrate ($Hg(NO_3)_2$), sodium nitrate ($NaNO_3$), copper nitrate ($Cu(NO_3)_2$), calcium nitrate ($Ca(NO_3)_2$), aluminum nitrate ($Al(NO_3)_3$), cesium nitrate ($Cs(NO_3)_2$), lead nitrate ($Pb(NO_3)_2$), and cobalt nitrate ($Co(NO_3)_2$) were purchased from Sigma Aldrich. Silver nitrate ($Ag(NO_3)_2$), sodium hydroxide (NaOH), and ammonia (NH_4) were purchased from Merck. All reagents were of analytical grade and were used without additional purification. All analyte solutions were prepared in Millipore ultrapure double-deionized water.

2.2. Instrumentation. The surface morphology of the prepared nanocomposite was studied using a high-resolution Carl Zeiss Gemini SEM500 electron microscope operating at an electron accelerating voltage of 6.0 kV and working distances of 4.1 and 4.3 mm (Carl Zeiss, Germany). X-ray diffraction (XRD) patterns were obtained on a D2 Phaser XRD-300 W powder diffractometer (Bruker, AXS GmbH, Karlsruhe, Germany) for a 2θ range of 10–90 at a scan rate of 0.05 degree/s using Cu Kα radiation at 40 kV and 100 mA. Raman spectra were measured by a Horiba LabRam Raman spectrometer equipped with a 785-nm laser line as an excitation source (Jobin–Yvon Technology, France) and a CCD detector. A Thermo-Fisher UV-visible absorbance spectrophotometer was used to collect UV-vis spectra using 1 cm glass cuvettes as sample cells. An Axis Supra X-ray Photoelectron Spectrometer (XPS) (Kratos Analytical, Manchester, UK) was used to assess the surface chemical composition of the Au@ZnO/Fe_3O_4 and confirm the formation of an amalgam when Hg^{2+} ions encountered Au.

2.3. Preparation of Fe_3O_4 Nanospheres. The Fe_3O_4 magnetic nanoparticles were prepared based on the co-precipitation of Fe^{3+} and Fe^{2+} under aqueous ammonia as a precipitating agent, with some modifications [60]. In brief, $FeSO_4.7H_2O$ (3.48 g) and $FeCl_3.6H_2O$ (3.38 g) were each dissolved in 100 mL of deionized water and mixed under vigorous stirring. Aqueous ammonia was dropped slowly into the solution. It was observed that the solution became black. The black mixture was then aged at 85°C for 2 h. After that, the product prepared was allowed to cool overnight. Finally, the black product was washed with deionized water and dried in the oven for 6 h at 70°C.

2.4. Preparation of the ZnO/Fe_3O_4 Composite. In preparing the ZnO/Fe_3O_4 composite, we employed a previously developed method with minor modifications [61]. In brief, 0.15 g of Fe_3O_4 was dispersed in 200 mL of 45 mM zinc nitrate solution. The mixture was then stirred to homogenize. Under vigorous stirring, to this mixture, at 70°C, 90 mM of NaOH solution was added slowly within 1 h. The reaction mixture was kept under stirring at 70°C for 2 h. Then, it was left at room temperature overnight to complete precipitation. Thereafter, the composite was cleaned repeatedly with deionized water and then separated from the water by using a ferromagnet and placed in an oven at a temperature of 70°C for 6 h to dry. After drying, the particles were annealed at a temperature of 350°C for 1 h.

2.5. Synthesis of Gold Nanoparticles on ZnO/Fe_3O_4 Composite. A simple but novel thermal method was employed to deposit gold nanoparticles on ZnO/Fe_3O_4 composites. In brief, 0.4 g of ZnO/Fe_3O_4 composite was dispersed in 5 mM of 50 mL $HAuCl_4$ solution (dissolved in ethylene glycol) and sonicated for 3 min to disperse the particles uniformly. The mixture was then placed in a water bath at 95°C for 20 min. The resulting gold-coated ZnO/Fe_3O_4 composites were then cleaned with deionized water and placed in the oven at 70°C for 3 h.

2.6. Catalytic Performance and Colorimetric Detection of Hg^{2+}. Initially, the catalytic activity of the Au@ZnO/Fe_3O_4 composites was investigated by using the reduction of 4-NP to 4-AP as a model reaction in the presence of freshly prepared $NaBH_4$ as the reducing agent. In a typical reaction, to a glass cuvette containing 3 mg of Au@ZnO/Fe_3O_4, 100 μL of deionized water and freshly prepared 0.1 mM of 1 mL 4-NP were added. To this reaction mixture, 1 mL of freshly prepared 100 mM $NaBH_4$ was added. Thereafter, the progress of the reduction reaction was monitored by measuring the absorbance of the reaction mixture using a UV/visible spectrophotometer in the range of 250–600 nm.

The detection of Hg^{2+} was assessed by studying the catalytic activity of Au@ZnO/Fe_3O_4 composite in the presence of varying Hg^{2+} concentrations. Here, 3 mg of Au@ZnO/Fe_3O_4 was incubated in 100 mL solution with different concentrations. Then, 1 mL of 4-NP solution (0.1 mM) was added to the solution and 1 mL of freshly prepared $NaBH_4$ solution (100 mM) was quickly added to the mixture. Then, the colorimetric reaction was allowed to proceed for 10 min. The resultant solution was scanned by a UV/Vis spectrophotometer with a wavelength range of 250–800 nm, and λ_{max} of 400 nm was used as the detection signal.

2.7. Sensitivity and Selectivity of the Au@ZnO/Fe_3O_4 Composite. To estimate the sensitivity and quantitative range of the Au@ZnO/Fe_3O_4 for the determination of Hg^{2+} ions, a range of varying concentrations of Hg^{2+} ions (0–20 nM) were added to the sensing solution, and absorbance variations at 400 nm were recorded. The selectivity of the AuNP@ ZnO/Fe_3O_4 system for Hg^{2+} ions detection was evaluated by monitoring the UV absorption response to interference metal ions including Ag^+, Na^+, Cu^{2+}, Mg^{2+}, Ca^{2+}, Al^{3+}, Cs^{2+}, Zn^{2+}, Pb^{2+}, Co^{2+}, and anion NO_3^- at a concentration of 20 μM.

3. Results and Discussion

3.1. Fabrication of Fe_3O_4, ZnO/Fe_3O_4, and $Au@ZnO/Fe_3O_4$. The fabrication of Fe_3O_4, ZnO/Fe_3O_4, and $Au@ZnO/Fe_3O_4$ was described in the sections mentioned above. Based on equation (1), the formation of a solid-state Fe_3O_4, as the only solid-state product meant that the black precipitate that was described above have formed on the addition of the precipitating agent, aqueous ammonia could be attributed to the Fe_3O_4 solid product in equation (1).

$$Fe^{2+}_{(aq.)} + 2Fe^{3+}_{(aq.)} + 8OH^{-}_{(aq)} \longrightarrow Fe_3O_{4\,(s)} + 4H_2O_{(l)}. \quad (1)$$

The separation of the black precipitate, Fe_3O_4 solid particles, by a ferromagnet confirmed the paramagnetism of Fe_3O_4 as has been reported elsewhere [62]. Thereafter, when the precipitate was dispersed in an alkaline zinc nitrate solution, a grey solid powder was formed. Based on equation (2) [63], the reaction involved a double exchange that occurred between $Zn(NO_3)_2$ and NaOH, resulting in the formation $Zn(OH)_2$, as the only solid-state product.

$$Zn\left(NO_2\right)_{3\,(aq.)} + Na\left(OH\right)_{(aq.)} \longrightarrow Zn\left(OH\right)_{2\,(S)} + NaNO_{3\,(aq.)}. \quad (2)$$

After annealing the grey solid powder, a brown solid powder was formed, and according to equation (3) [63], during the annealing process, zinc hydroxide had decomposed into zinc oxide.

$$Zn\left(OH\right)_{2\,(S)} \longrightarrow ZnO_{(S)} + H_2O_{(g)}. \quad (3)$$

The brown solid powder formed during annealing was attracted to a ferromagnet; this in addition confirmed that, a composite of ZnO and Fe_3O_4 which we named, ZnO/Fe_3O_4 had been formed and the paramagnetism of the Fe_3O_4 was retained. Finally, a brick-red composite was formed when the brown composite was reacted with auric acid in ethylene glycol at slightly high temperatures, via the polyol synthesis method. The brick-red composite which we named $Au@ZnO/Fe_3O_4$ was also attracted to a ferromagnet, confirming that the paramagnetism of the Fe_3O_4 was still retained. The fabrication of Fe_3O_4, ZnO/Fe_3O_4, and $Au@ZnO/Fe_3O_4$ was confirmed by characterizing for size, shape, morphology, crystallinity, and surface chemistry.

3.2. SEM Characterization. The sizes, shapes, and morphologies of the prepared black precipitate attributed to Fe_3O_4, brown powder attributed to ZnO/Fe_3O_4, and brick-red fine particles attributed to $Au@ZnO/Fe_3O_4$ composite were obtained using SEM. The SEM micrograph for Fe_3O_4 displayed spherical particles that were mostly agglomerated (see Figure 1(a)), with an average individual particle diameter of 26 nm measured using image J software (see Figure 1(d)). The nanosize diameter confirmed the nanoparticulate nature of the prepared Fe_3O_4 black precipitate. Our findings were supported by the work of Ba-Abbad et al. [64], where they reported that using ammonia as a precipitating agent resulted in spherically shaped Fe_3O_4 nanoparticles (NP), whereas using NaOH resulted in cubic-shaped NPs. They concluded that the formation of Fe_3O_4 NPs relied on the type of precipitating agent. Independently, Mazhani et al. [65] and Petcharoen and Sirivat [66] also synthesized Fe_3O_4 via the coprecipitation method using ammonia as a precipitating agent and similarly, their SEM imaging showed that they had produced spherical shaped Fe_3O_4 NPs. The referenced research works supported the nanosize and spherical shape of Fe_3O_4 particles that we also obtained, with ammonia as the precipitating agent.

Figure 1(b) displays the SEM micrograph of the brown ZnO/Fe_3O_4 composite. It displays irregular shapes of what looks like broken monoliths. Figure 1(c) is a SEM micrograph of the brick-red fine solid particles of $Au@ZnO/Fe_3O_4$ composite. According to Holade et al. [67], it displays scarcely dispersed nanoparticles of different sizes and shapes coated on top of the ZnO/Fe_3O_4 monoliths.

The reduction of auric acid by ethylene glycol takes place simultaneously with the oxidation of ethylene glycol, with several possible oxidation pathways and products (aldehydes, carboxylic acids, or CO_2) forming, depending on the temperature, pH, and chemical environment. As already established, the shapes of the nanoparticles formed are determined by the rate at which metal atoms add to metal clusters (fluxional assemblies) to form seeds (nonfluxional), the structures of these initial seeds (twinned vs single crystal), the rate at which metal atoms add to seed faces, and the binding selectivity of capping agents. The rates at which metal atoms form and assemble are sensitive to reduction kinetics, which in turn are dependent on the reductant [68]. Therefore, we believe that the combination of moderately high reaction temperature, the solution pH, and ZnO/Fe_3O_4 and $Au@ZnO/Fe_3O_4$ possibly acting as catalysts in the oxidation of ethylene glycol may have resulted in the formation of different oxidation products or all the possible oxidation products as reductants of Au (III) to Au(0), hence the formation of different sizes and shapes of Au (0).

3.3. XRD Characterization. Analysis through X-ray diffraction spectrophotometry was carried out to confirm the crystalline nature of the fabricated particles. The X-ray diffraction (XRD) pattern marked Fe_3O_4 shown in Figure 2 exhibited 2θ peaks at 30.20°, 35.45°, 43.25°, 53.55°, 56.78°, and 62.73° marked with indices at (220), (211), (400), (422), (511), and (400) (JCPDS no. 19-0629), respectively. The peak positions and intensities matched well with those reported before for the inverse spinel structure of magnetite [69, 70] and have been reported to show the face-centered cubic structure of Fe_3O_4 [71]. Crystallographically, magnetite takes on a cubic inverse spinel structure due to the fact that the oxide ions form a face-centered cubic, with the iron (II) and iron (III) cations occupying one-eighth of the tetrahedral and half of the octahedral holes, respectively [72].

Furthermore, on the XRD pattern marked ZnO/Fe_3O_4 in Figure 2, the peaks at 2θ 31.77°, 34.42°, 36.25°, 47.54°, 56.60°, 62.86°, 66.38°, 67.96°, and 69.10° corresponding to (100), (002), (101), (102), (110), (103), (200), (112), and (201) (JCPDS no. 36-1451), respectively, were observed. The

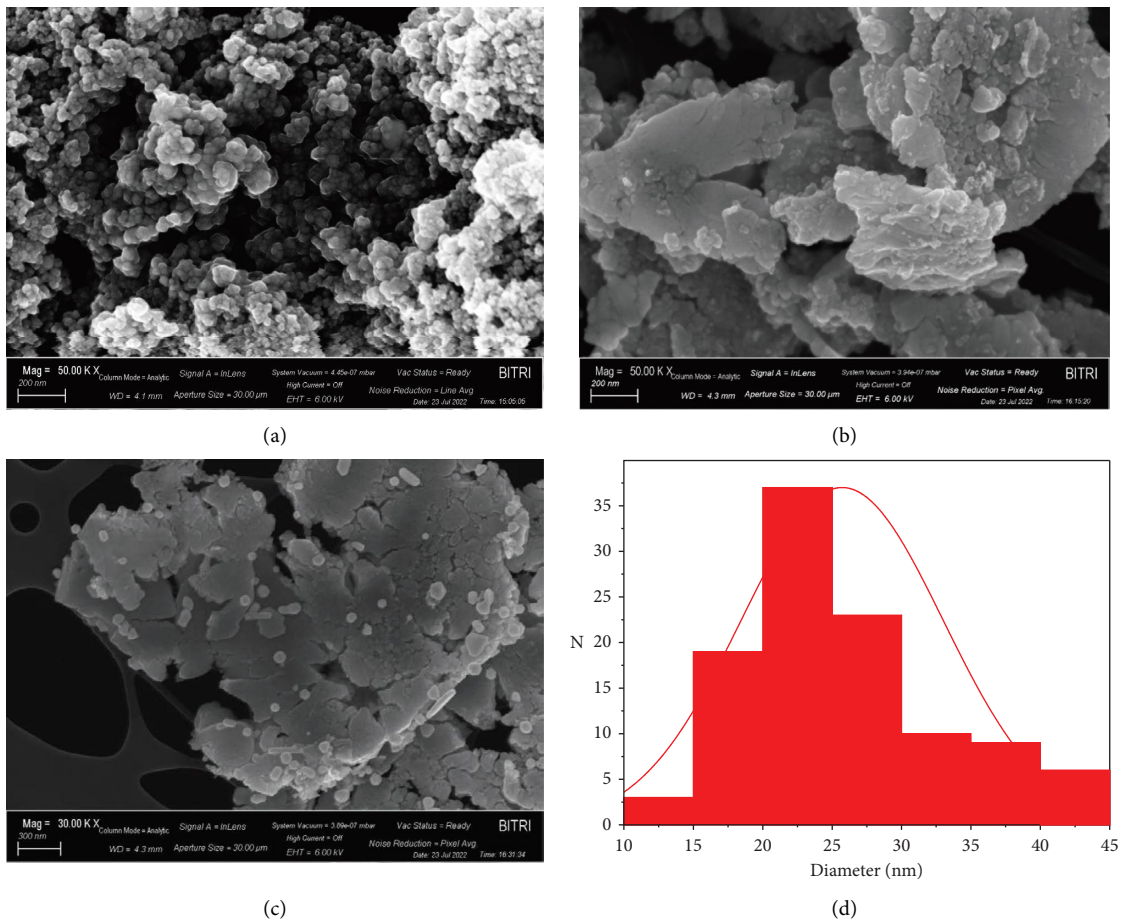

Figure 1: SEM images of (a) Fe_3O_4, (b) ZnO/Fe_3O_4, and (c) $Au@ZnO/Fe_3O_4$ nanostructures, (d) particle size distribution of Fe_3O_4.

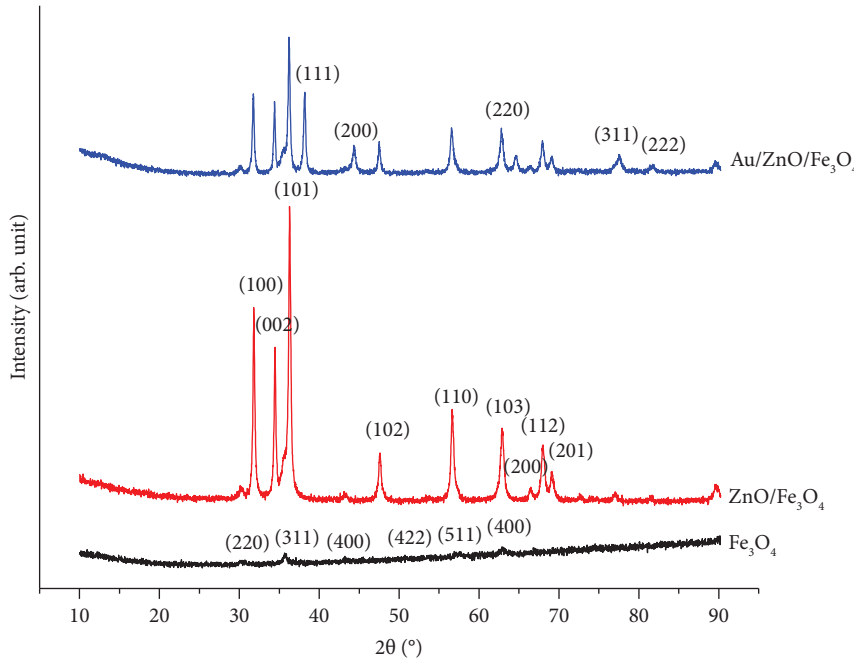

Figure 2: XRD patterns of Fe_3O_4, ZnO/Fe_3O_4, and $Au@ZnO/Fe_3O_4$.

positions and relative intensities of the diffraction peaks matched well with those reported before for hexagonal zincite-type of structure [73, 74] which indicated the formation of a highly crystalline ZnO structure [58]. In this pattern, in addition to the peaks assigned to ZnO, peaks at 2θ 30.20°, 35.45°, 43.25°, 53.55°, 56.78°, and 62.73° marked with indices at (220), (211), (400), (422), (511), and (400) previously attributed to cubic spinel structured magnetite were observed in the nanocomposites, revealing that the phases of Fe_3O_4 nanocrystals did not change; furthermore, this confirmed the formation of ZnO/Fe_3O_4 composites.

Finally, on the XRD pattern marked Au@ ZnO/Fe_3O_4, five strong peaks that were not observed for ZnO/Fe_3O_4 composite appeared. The peaks were observed at diffraction angles of 38.20°, 44.40°, 64.60°,77.60°, and 81.76° with the indices (111), (200), (220), (311), and (222) (JCPDS no. 04-0784), respectively. The peaks have been attributed to the Au crystal with a cubic phase [75, 76]. The peaks attributed to the ZnO structure still appeared on this pattern. The XRD results clearly indicated the successful synthesis of Au@ ZnO/Fe_3O_4 hybrid materials.

3.4. Raman Characterization. The formation of gold nanoparticles on the surface of ZnO/Fe_3O_4 was confirmed by surface-enhanced Raman spectroscopy (SERS). Gold nanoparticles can produce ultrasensitive surface-enhanced Raman scattering (SERS) signals owing to their plasmonic properties. Collective oscillation of free electrons on the surface of gold nanoparticles enhances the Raman signal of molecules which are adsorbed or are in close proximity to gold nanoparticles [77]. The mechanism relevant to SERS is the surface enhancement of the electromagnetic field at the interface between the SERS active substrate (e.g., gold) and a molecule of interest through resonant excitation of surface plasmons of the metal [78]. This mechanism was exploited to confirm the formation of AuNPs on the surface of ZnO/Fe_3O_4. SERS effect of the nanostructures was investigated using 4-nitrothiophenol (4-NTP) as a probe molecule because of its strong Raman activity and strong affinity to chemisorption on gold surfaces [79]. The synthesized Fe_3O_4, ZnO/Fe_3O_4, and Au@ ZnO/Fe_3O_4 particles were soaked in 1 mM of 4-NTP for 1 h to allow for chemisorption of the 4-NTP on the surface of the nanoparticles and then air dried before SERS analysis. The SERS spectrum in Figure 3 representing the measured conditions for Au@ ZnO/Fe_3O_4 showed bands at 1567 cm^{-1}, 1336 cm^{-1}, 1110 cm^{-1}, 1075 cm^{-1}, 854 cm^{-1}, and 722 cm^{-1} for 4-nitrothiophenol. These could be attributed to the benzene ring C = C stretching, symmetrical NO_2 stretching, C-H bending vibration, in-plane C-S stretching modes, C-H wagging vibrations, and C-S wagging vibrations, respectively [65, 80, 81]. On the other hand, Raman scattering was not observed under the measured conditions for ZnO/Fe_3O_4 and Fe_3O_4 as shown in Figure 3(ii) and (iii), respectively, indicating that the particles did not exhibit any SERS effect. This served as confirmation that gold nanoparticles were formed on the surface of ZnO/Fe_3O_4.

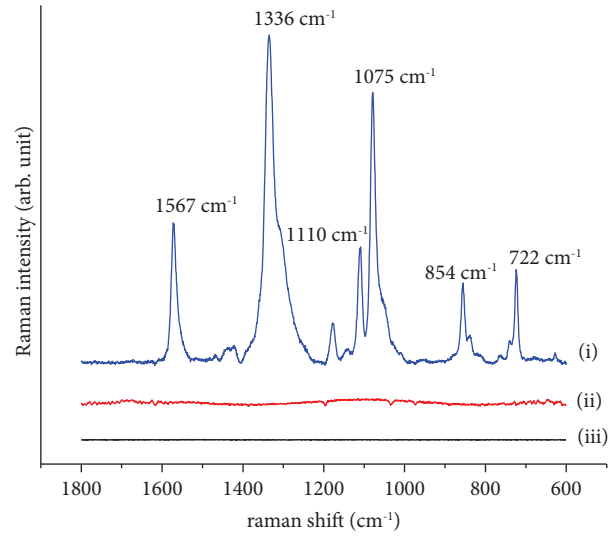

FIGURE 3: SERS spectra of pNTP with (i) Au@ZnO/Fe_3O_4 (ii) ZnO/Fe_3O_4, and (iii) Fe_3O_4 as SERS substrates.

3.5. XPS Characterization. XPS analysis was carried out to assess the surface chemical composition of the Au@ZnO/Fe_3O_4. The XPS spectrum in Figure 4(a) shows overlapping peaks. Upon deconvolution, it resolved into four peaks at binding energies of 92 eV, 89 eV, 88 eV, and 85 eV. These peaks were attributed to Zn $3p_{1/2}$, Zn $3p_{3/2}$, Au $4f_{5/2}$, and Au $4f_{7/2}$, respectively [82]. The spectrum obtained confirmed the formation of AuNP on the surface of ZnO NP.

The XPS spectrum in Figure 4(b) shows two binding-energy peaks at 101.64 eV and 105.64 eV that were formed by the addition of Hg^{2+}. The peaks were ascribed to Hg $4f_{5/2}$ and Hg $4f_{7/2}$, respectively [27], which revealed that Hg^0 was formed on the surface of Au@ZnO/Fe_3O_4, confirming the formation on an Au-Hg amalgam on the surface of Au@ ZnO/Fe_3O_4 as has been reported by Long et al. [46, 83] in the past. In the same study, Long et al. further reported that the existence of Hg^0 on the surface of AuNPs had great influence on the features of the surface of AuNPs, including adsorption on the surface of AuNPs.

3.6. Construction of the Nanoprobe and Detection of Hg^{2+}. The excellent qualities of the different components that constituted the prepared catalytic hybrid material, Au@ ZnO/Fe_3O_4 allowed versatility in the design and tailoring of a multifunctional material with distinct properties that were brought about by the combined effect of the traits of the individual components. For instance, the prepared Fe_3O_4 nanoparticles provided the magnetic separation property; however, the ferromagnetic NPs aggregated too easily due to their magnetic dipole-dipole interactions and decreased the efficiency of the catalytic property of NPs [27]. Also, according to Chen et al. [84], it is notably difficult to directly attach AuNPs to the surfaces of the Fe_3O_4 owing to the dissimilar nature of the two species' surfaces. To deal with this challenge, we successfully used ZnO NPs to facilitate the formation of AuNP on the

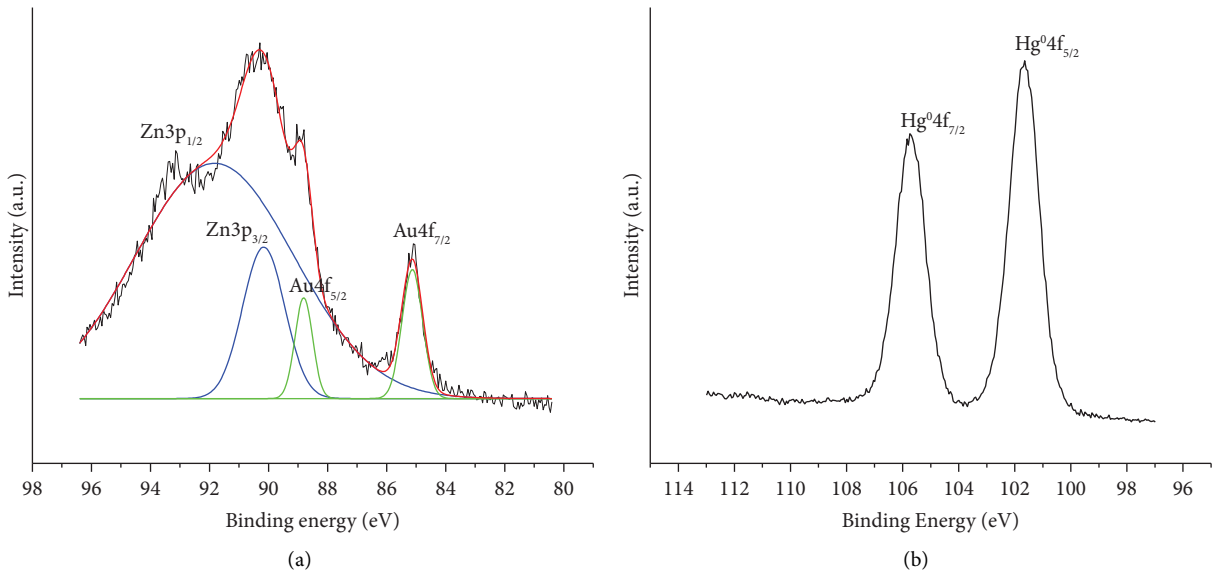

Figure 4: XPS spectra of Au@ZnO/Fe_3O_4 (a) before and (b) after interaction with Hg^{2+}.

nanomaterial because of the closeness of intrinsic absorption and emission bands of ZnO with the surface plasmon peak of Au at resonant coupling.

In this work, the reduction of 4-nitrophenol to 4-aminophenol in the absence and presence of the prepared Au@ZnO/Fe_3O_4 as a catalyst as well as in the absence and presence of Hg^{2+} as the analyte of interest, was monitored via UV-visible spectroscopy which showed differences in absorbance intensities at lambda max = 400 nm in the different reaction systems (see Figure 5). Figure 5(i) shows that the recorded absorbance for the reduction of 4-nitrophenol by excess $NaBH_4$ solution in the absence of the catalyst was highest and was found to be lowest in the presence of the catalyst (see Figure 5(ii)). In the presence of the catalyst, AuNPs acted as electron relay centers and initiated the shifting of electrons from the donor, BH_4^- to the acceptor, 4-nitrophenol. The reacting molecules (BH_4^- ion and 4-nitrophenol) were simultaneously adsorbed onto the surface of the NPs. As a result, electrons were transferred from the BH_4^- ion to 4-nitrophenol through the NPs, causing the fast reduction of 4-nitrophenol to 4-aminophenol [85] and the lowest absorbance was recorded. Without the catalyst, the reduction of 4-nitrophenol by excess $NaBH_4$ was very slow hence very little 4-nitrophenol was converted to 4-aminophenol and the absorbance was the highest.

However, when Hg^{2+} was added to the system (see Figure 5(iii)), the absorbance at 400 nm was reduced but only to a lesser extent compared to when Hg^{2+} was not added to the system (Figure 5(ii)), depicting a decrease in the catalytic activity of Au@ZnO/Fe_3O_4. This reduction in catalytic activity was because of the inhibition caused by the formation of gold-hydride species by the resulting Au-Hg amalgam formed, leading to the slow reduction of 4-nitrophenol to 4-aminophenol. The formation of Au-Hg amalgam which causes the slow reduction of 4-nitrophenol to 4-aminophenol has also been reported before by He and Zheng [86]. It should be noted that the observations in Figure 5 were accompanied by color changes. The reaction system attributed to the reduction of 4-nitrophenol by excess $NaBH_4$ in the absence of the catalyst represented by the spectrum in Figure 5(i) was bright yellow in color and then when the catalyst was added to the system represented by the spectrum in Figure 5(ii) the solution changed to colourless and finally, when mercury was added to the system represented by the spectrum in Figure 5(iii) the solution only changed to pale yellow. The color changes, with further investigations, may be employed in the colorimetric screening of Hg^{2+}.

3.7. Optimization of Parameters on the Detection of Hg^{2+}. The incubation time for the colorimetric screening of Hg^{2+} via the catalytic reduction of 4-nitrophenol to 4-aminophenol was studied in the absence and presence of mercury in order to identify the best time at which the reaction occurs. The results are shown in Figure 6.

The spectra in Figures 6(a) and 6(b) show a decrease in the absorption signal at lambda max = 400 nm with increasing time both in the absence and presence of Hg^{2+}, respectively, signaling the reduction of 4-nitrophenol to 4-aminophenol with time. This reaction was slower in the presence of Hg^{2+} than in its absence, due to an increase in the quantity of Au-Hg amalgam formed with the increase in time. The experiment was stopped at 20 mins since there was no discernible absorbance peak at lambda max = 400 nm in the absence of Hg^{2+}. From the spectra in Figure 6(a), it was concluded that a reasonable time at which this experiment could be carried out showing discernible peaks was at any time between 8 and 12 min. Thus, for our work, 10 mins was chosen as the optimal time. It should be noted that there were corresponding color changes with time that were also observed.

The effect of the concentration of 4-nitrophenol on the absorbance signal was also studied. The results are shown in Figure 7.

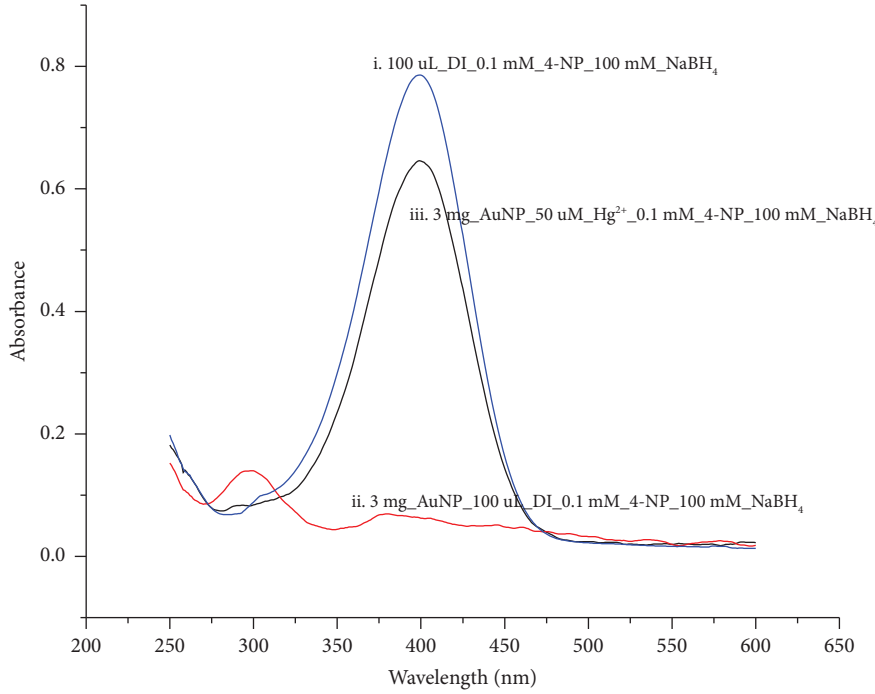

FIGURE 5: UV-vis absorbance spectra showing the effect of the catalyst and Hg^{2+} on the reduction of 4-nitrophenol to 4-aminophenol.

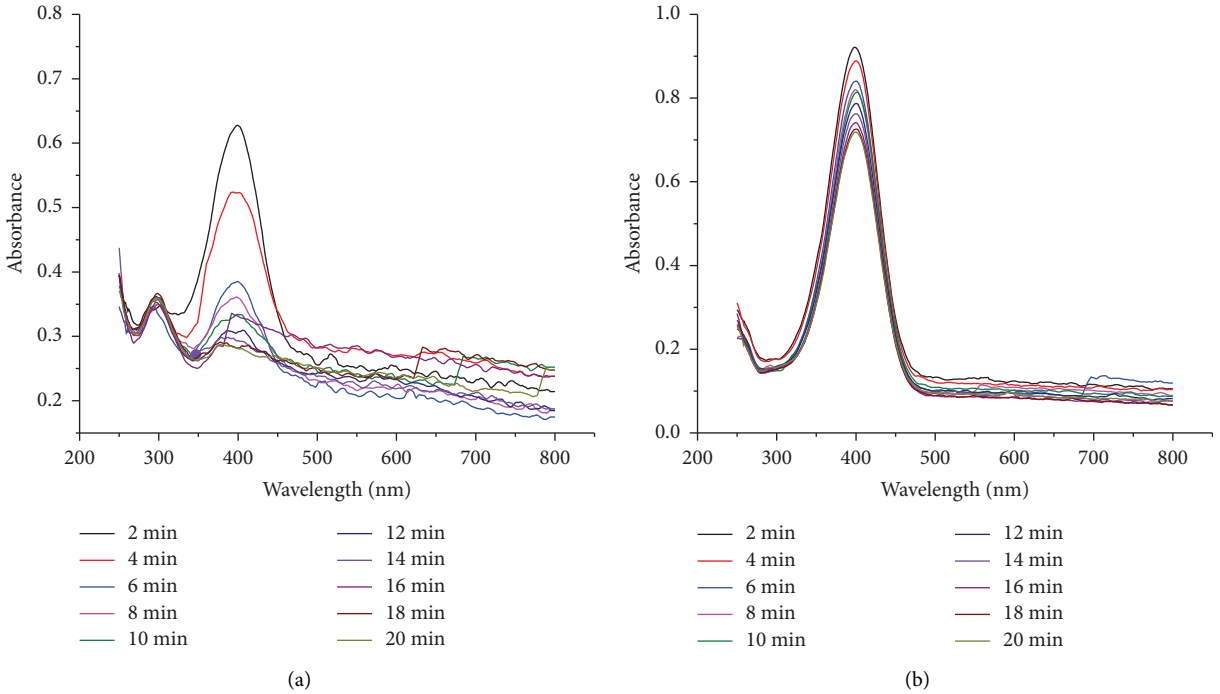

FIGURE 6: The effect of incubation time on the response signal; spectra showing the effect of incubation time on the response signal of 0.1 mM of 4-nitrophenol in the sensing system at 400 nm (a) before and (b) after adding mercury.

As depicted by the spectra in Figures 7(a) and 7(b), the absorbance increased with increasing concentration of 4-nitrophenol at optimal 10 min incubation time, both in the absence and presence of Hg^{2+}, respectively. In both cases, there were more 4-nitrophenol molecules in the system available to be reduced, hence the increase in absorbance with increasing concentrations of 4-nitrophenol. There were discernible peaks at all concentration levels, therefore any of the concentrations of 4-nitrophenol studied was suitable for the colorimetric screening of Hg^{2+} to give distinct color changes. Thus, for this work 0.05 mM of 4-nitrophenol was used.

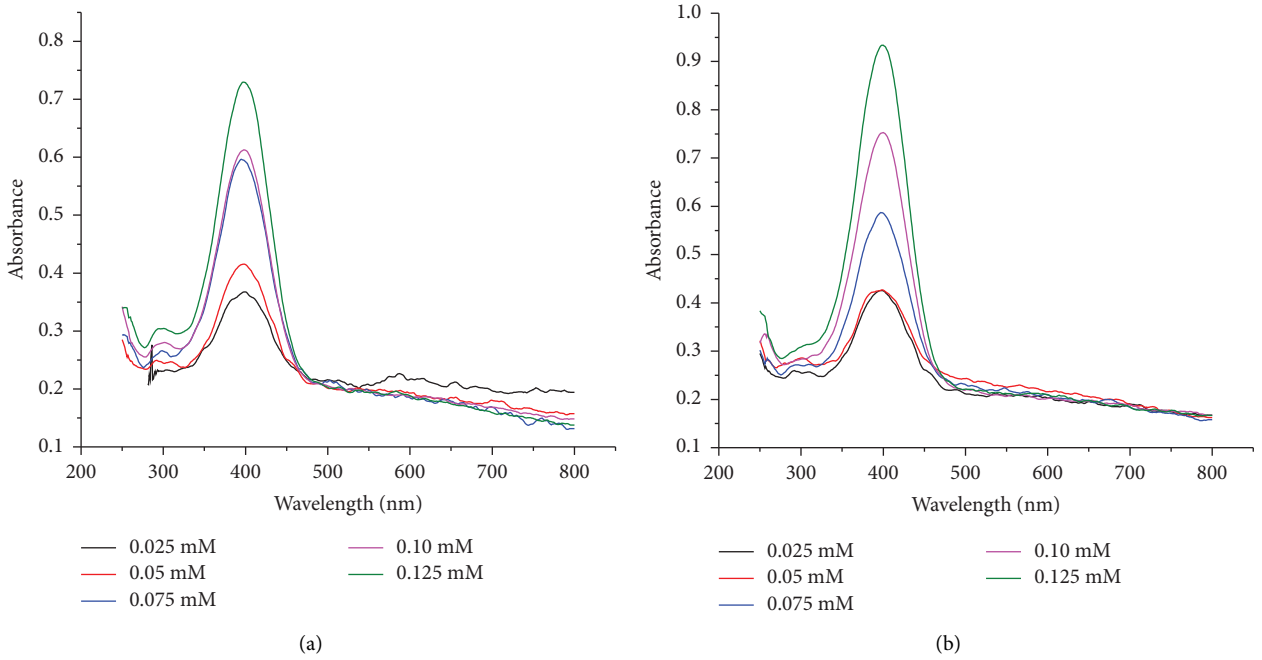

FIGURE 7: The effect of the amount of 4-nitrophenol on the response signal; spectra showing the effect of varying concentrations of 4-nitrophenol on the response signal (a) before and (b) after adding mercury.

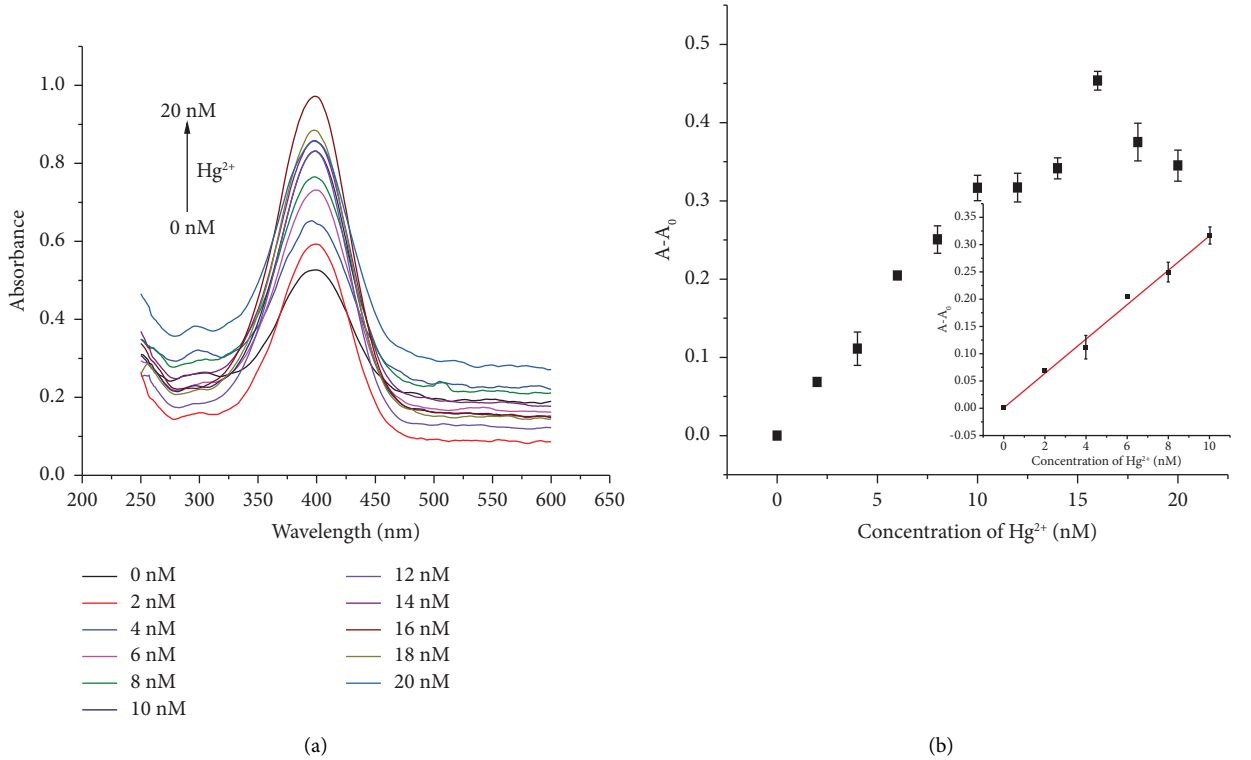

FIGURE 8: Sensitivity of Au@ZnO/Fe_3O_4 towards Hg^{2+}. (a) Absorption spectra of 4-NP under varying concentrations of Hg^{2+} (0–20 nM). (b) Calibration curve of absorbance variation versus the concentration of Hg^{2+} added (the linear relationship between absorption signal and Hg^{2+} concentration.).

Table 1: Comparison of the proposed method with other reported Au-based nanoenzymes for the detection of Hg^{2+}.

Material	Method	Linear range (nM)	Detection limit (nM)	Ref
AuNP@MOF	Reductase mimetic	0.2–0.4	0.10	[26]
AuNP	Reductase mimetic	0–10	1.45	[36]
Au@ZnO/Fe_3O_4	Reductase mimetic	0–10	2.34	This work
Fe_3O_4@ZnO	Peroxidase mimetic	0–10	23	[69]
Cs-AuNP	Peroxidase mimetic	0–200	20	[34]

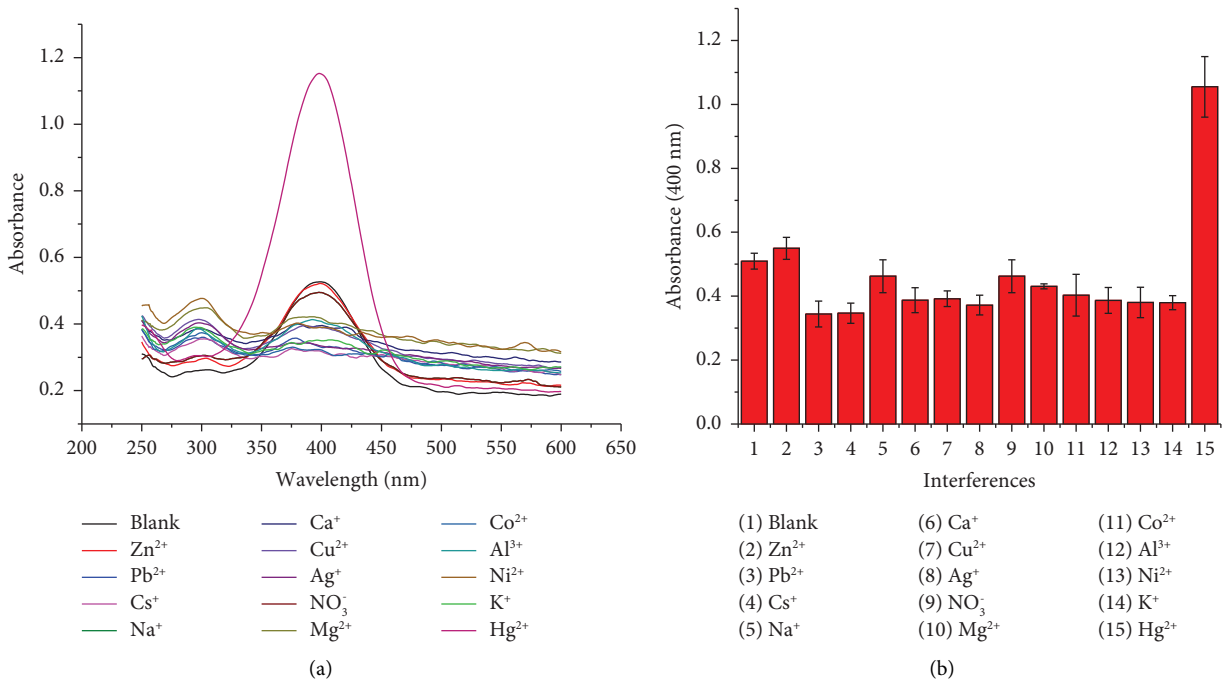

Figure 9: Selectivity of Au@ZnO/Fe_3O_4 towards Hg^{2+}. (a) Absorption spectra of 4-NP in the presence of Hg^{2+} and possible competing species. (b) Bar graph comparing absorbances of possible interferents to Hg^{2+}.

Table 2: The detection of Hg^{2+} in a cosmetic product.

Spiking concentration (nM)	Detected concentration (nM)	Recovery (%)	RSD (%)
4.00	4.01	100.29	13.83
6.00	5.93	98.78	7.96
8.00	7.72	96.49	4.26

3.8. Sensitivity and Selectivity in the Determination of Hg^{2+}. Figure 8(a) shows the absorbance spectra of Hg^{2+} from 0 to 20 nM. It was found that the absorbance at 400 nm increased with increasing concentration of Hg^{2+} until 16 nM then began to decrease. Figure 8(b) presents the absorbance signal difference as a function of Hg^{2+} concentration. The absorbance signal was linearly related to Hg^{2+} concentration in the range of 0–10 nM. The LOD of the colorimetric sensor is calculated by using the following equation: $\mathrm{LOD} = 3\sigma/k$, where k is the slope of the calibration curve and σ is the standard deviation of the blank solution of 4-NP absorbances recorded. It was calculated to be as low as 2.34 nM. Compared to other colorimetric methods employing Au-based nanoenzymes (Table 1), the currently proposed method fairs well. Not only does it offer high sensitivity and fast response, but it is also convenient and stable.

In addition to sensitivity, selectivity is also a critical parameter to evaluate the performance of an assay. The unique affinity of Hg^{2+} towards Au provided excellent selectivity towards detecting other potentially interfering metal ions. Figures 9(a) and 9(b) show that other metal ions including Ag^{+}, Na^{+}, Cu^{2+}, Mg^{2+}, Ca^{2+}, Cs^{2+}, Zn^{2+}, Pb^{2+}, Co^{2+}, Al^{3+}, K^{+}, and Ni^{2+} do not have the ability to suppress the catalytic reduction of 4-NP by Au@ZnO/Fe_3O_4, instead they seem to enhance it at double the concentration of Hg^{2+}.

3.9. Determination of Mercury-Spiked Real Samples. The performance of the proposed colorimetric method was evaluated for the determination of mercury in a cosmetic product purchased locally. The results are summarized in Table 2. As shown in Table 2, the recoveries are in the range

of 96.5–100.3% and the RSD is in the range of 4.3–13.8% for $n = 3$. This indicates that the proposed method has a high accuracy and reliability for the analysis of Hg^{2+} in real samples.

4. Conclusion

In summary, we have successfully developed a high-performance colorimetric probe for the detection of Hg^{2+} ions based on the inhibition of the catalytic activity of Au@ ZnO/Fe_3O_4 on the borohydride reduction of 4-NP. The probe is simple, rapid, sensitive, and selective. It can sensitively detect Hg^{2+} with LODs of 2.34 nM. The colorimetric change is obvious and allows one to recognize the color change at low Hg^{2+} concentrations. Its excellent selectivity is owed to the gold amalgam process that occurs specifically between Au and Hg. The magnetic core allows for convenient separation during analysis. Moreover, the probe has shown great potential for the accurate detection of Hg^{2+} in a skin-lightening cosmetic product.

Data Availability

The data used to support the findings of this study are available from the corresponding author upon request.

Conflicts of Interest

The authors declare that they have no conflicts of interest.

Acknowledgments

This work was supported by the Office of Research, Development, and Innovation (ORDI), Botswana International University of Science and Technology.

References

[1] E. Dhia, "H Osman, and A Dahab. Investigation of mercury content in cosmetic products by using direct mercury analyzer," *American Journal of PharmTech Research*, vol. 5, no. 5, pp. 205–212, 2015.

[2] European Union, "Compilation of submission on Cosmetics," 2022.

[3] FDA's Testing of Cosmetics for Arsenic, "Cadmium, chromium, cobalt," 2022.

[4] Y. Gao, Z. Shi, Q. Zong, P. Wu, J. Su, and R. Liu, "Di- rect determination of mercury in cosmetic samples by isotope dilution induc- tively coupled plasma mass spectrometry after dissolution with formic acid," *Analytica Chimica Acta*, vol. 812, pp. 6–11, 2014.

[5] J. H. An, S. J. Park, O. S. Kwon, J. Bae, and J. Jang, "High-performance flexible graphene aptasensor for mercury detection in mussels," *ACS Nano*, vol. 7, no. 12, pp. 10563–10571, 2013.

[6] A. Coskun, M. D. Yilmaz, and E. U. Akkaya, "Bis (2-pyridyl)-substituted boratriazaindacene as an NIR-emitting chemosensor for Hg (II)," *Organic Letters*, vol. 9, no. 4, pp. 607–609, 2007.

[7] Y. Ding, S. Wang, J. Li, and L. Chen, "Nanomaterial- based optical sensors for mercury ions," *TrAC, Trends in Analytical Chemistry*, vol. 82, pp. 175–190, 2016.

[8] A. Coskun and E. U. Akkaya, "Signal ratio amplification via modulation of resonance energy transfer: proof of principle in an emission ratiometric Hg (II) sensor," *Journal of the American Chemical Society*, vol. 128, no. 45, pp. 14474-14475, 2006.

[9] S. K. Ko, Y. K. Yang, J. Tae, and I. Shin, "In vivo monitoring of mercury ions using a rhodamine-based molecular probe," *Journal of the American Chemical Society*, vol. 128, no. 43, pp. 14150–14155, 2006.

[10] T. Lou, Z. Chen, Y. Wang, and L. Chen, "Blue-to- red colorimetric sensing strategy for Hg^{2+} *and* Ag^{+} via redox-regulated sur- face chemistry of gold nanoparticles," *ACS Applied Materials & Interfaces*, vol. 3, no. 5, pp. 1568–1573, 2011.

[11] K. Nie, B. Dong, H. Shi, Z. Liu, and B. Liang, "Dike- topyrrolopyrrole amphiphile-based micelle-like fluorescent nanoparticles for selective and sensitive detection of mercury (II) ions in water," *Analytical Chemistry*, vol. 89, no. 5, pp. 2928–2936, 2017.

[12] T. Tolessa, Z. Q. Tan, Y. G. Yin, and J. F. Liu, "Single- drop gold nanoparticles for headspace microextraction and colorimetric assay of mercury (II) in environmental waters," *Talanta*, vol. 176, pp. 77–84, 2018.

[13] H. Wang, Y. Wang, J. Jin, and R. Yang, "Gold nanoparticle-based colorimetric and "turn-on" fluorescent probe for mercury (II) ions in aqueous solution," *Analytical Chemistry*, vol. 80, no. 23, pp. 9021–9028, 2008.

[14] J. Zang, C. Li, K. Zhou et al., "Nanomolar Hg^{2+} detection using β-lactoglobulin- stabilized fluorescent gold nanoclusters in beverage and biological media," *Analytical Chemistry*, vol. 88, no. 20, pp. 10275–10283, 2016.

[15] D. Li, A. Wieckowska, and I. Willner, "Optical analysis of Hg^{2+} ions by oligonucleotide–gold-nanoparticle hybrids and DNA-based machines," *Angewandte Chemie*, vol. 120, no. 21, pp. 3991–3995, 2008.

[16] A. Ono and H. Togashi, "Highly selective oligonucleotide-based sensor for mercury (II) in aqueous solutions," *Angewandte Chemie*, vol. 116, no. 33, pp. 4400–4402, 2004.

[17] M. Pandeeswar, S. P. Senanayak, and T. Govindaraju, "Nanoarchi- tectonics of small molecule and DNA for ultrasensitive detection of mercury," *ACS Applied Materials & Interfaces*, vol. 8, no. 44, pp. 30362–30371, 2016.

[18] M. Hollenstein, C. Hipolito, C. Lam, D. Dietrich, and D. M. Perrin, "A highly selective dnazyme sensor for mercuric ions," *Angewandte Chemie*, vol. 120, no. 23, pp. 4418–4422, 2008.

[19] J. Liu and Y. Lu, "Rational design of "turn-on" allosteric dnazyme cat- alytic beacons for aqueous mercury ions with ultrahigh sensitivity and selec- tivity," *Angewandte Chemie International Edition*, vol. 46, no. 40, pp. 7587–7590, 2007.

[20] P. Chen and C. He, "A general strategy to convert the merR family proteins into highly sensitive and selective fluorescent biosensors for metal ions," *Journal of the American Chemical Society*, vol. 126, no. 3, pp. 728-729, 2004.

[21] G. Henkel and B. Krebs, "Metallothioneins: zinc, cadmium, mercury, and copper thiolates and selenolates mimicking protein active site features- structural aspects and biological implications," *Chemical Reviews*, vol. 104, no. 2, pp. 801–824, 2004.

[22] G. Sener, L. Uzun, and A. Denizli, "Lysine-promoted colorimetric response of gold nanoparticles: a simple assay for ultrasensitive mercury (II) detection," *Analytical Chemistry*, vol. 86, no. 1, pp. 514–520, 2014.

[23] J. Hai, F. Chen, J. Su, F. Xu, and B. Wang, "Porous wood members-based amplified colorimetric sensor for Hg^{2+} detection through Hg^{2+}-triggered methylene blue reduction reactions," *Analytical Chemistry*, vol. 90, no. 7, pp. 4909–4915, 2018.

[24] K. N. Han, J. S. Choi, and J. Kwon, "Gold nanozyme-based paper chip for colorimetric detection of mercury ions," *Scientific Reports*, vol. 7, no. 1, pp. 1–7, 2017.

[25] R. Liu, L. Zuo, X. Huang et al., "Colorimetric determination of lead (II) or mercury (II) based on target induced switching of the enzyme-like activity of metallothionein- stabilized copper nanoclusters," *Microchimica Acta*, vol. 186, no. 4, pp. 250–258, 2019.

[26] X. Wang, H. Wang, L. Guo et al., "Colorimetric detection of Hg(ii) based on the gold amalgam-triggered reductase mimetic activity in aqueous solution by employing AuNP@MOF nanoparticlesAuNP@MOF nanoparticles," *The Analyst*, vol. 145, no. 4, pp. 1362–1367, 2020.

[27] S. Zhang, H. Li, Z. Wang et al., "A strongly coupled Au/Fe_3O_4/GO hybrid material with enhanced nanozyme activity for highly sensitive colorimetric detection, and rapid and efficient removal of Hg^{2+} in aqueous solutions," *Nanoscale*, vol. 7, no. 18, pp. 8495–8502, 2015.

[28] Z. Chen, C. Zhang, Y. Tan et al., "Chitosan-functionalized gold nanoparticles for colorimetric detection of mercury ions based on chelation- induced aggregation," *Microchimica Acta*, vol. 182, no. 3-4, pp. 611–616, 2015.

[29] J. Duan, H. Yin, R. Wei, and W. Wang, "Facile colori- metric detection of Hg^{2+} based on anti-aggregation of silver nanoparticles," *Biosensors and Bioelectronics*, vol. 57, pp. 139–142, 2014.

[30] C. Jiang, Z. Guan, S. Y. Rachel Lim, L. Polavarapu, and Q.-H. Xu, "Two-photon ratiometric sensing of Hg^{2+} by using cysteine functionalized Ag nanoparticles," *Nanoscale*, vol. 3, no. 8, pp. 3316–3320, 2011.

[31] C. W. Lien, Y. T. Tseng, C. C. Huang, and H. T. Chang, "Logic control of enzyme-like gold nanoparticles for selective detection of lead and mercury ions," *Analytical Chemistry*, vol. 86, no. 4, pp. 2065–2072, 2014.

[32] Z. Chen, C. Zhang, Q. Gao, G. Wang, L. Tan, and Q. Liao, "Colorimetric signal amplification assay for mercury ions based on the catalysis of gold amalgam," *Analytical Chemistry*, vol. 87, no. 21, pp. 10963–10968, 2015.

[33] Y. Q. Huang, S. Fu, Y. S. Wang et al., "Protamine-gold nanoclusters as peroxidase mimics and the selective enhancement of their activity by mercury ions for highly sensitive colorimetric assay of Hg (II)," *Analytical and Bioanalytical Chemistry*, vol. 410, no. 28, pp. 7385–7394, 2018.

[34] C. Jiang, Z. Li, Y. Wu, W. Guo, J. Wang, and Q. Jiang, "Colorimetric detection of Hg^{2+} based on enhancement of peroxidase- like activity of chitosan-gold nanoparticles," *Bulletin of the Korean Chemical Society*, vol. 39, no. 5, pp. 625–630, 2018.

[35] W. Li, Y. Li, H. L. Qian, X. Zhao, C. X. Yang, and X. P. Yan, "Fabrication of a covalent organic framework and its gold nanoparticle hybrids as stable mimetic peroxidase for sensitive and selective colorimetric detection of mercury in water samples," *Talanta*, vol. 204, pp. 224–228, 2019.

[36] Y. J. Long, Y. F. Li, Y. Liu, J. J. Zheng, J. Tang, and C. Z. Huang, "Visual observation of the mercury-stimulated peroxidase mimetic ac- tivity of gold nanoparticles," *Chemical Communications*, vol. 47, no. 43, pp. 11939–11941, 2011.

[37] C. Ma, Y. Ma, Y. Sun et al., "Colorimetric determination of Hg2+ in environmental water based on the Hg2+-stimulated peroxidase mimetic activity of MoS2-Au composites2+ in environmental water based on the Hg2+-stimulated peroxidase mimetic activity of MoS2-Au composites," *Journal of Colloid and Interface Science*, vol. 537, pp. 554–561, 2019.

[38] C. F. Peng, N. Pan, Z. J. Xie, and L. L. Wu, "Highly sensi- tive and selective colorimetric detection of Hg^{2+} based on the separation of Hg^{2+} and formation of catalytic DNA-gold nanoparticles," *Analytical Methods*, vol. 8, no. 5, pp. 1021–1025, 2016.

[39] Y. Wang, Y. Wang, F. Wang et al., "Electrochemical aptasensor based on gold modified thiol graphene as sensing platform and gold-palladium modified zirconium metal-organic frameworks nanozyme as signal enhancer for ultrasensitive detection of mercury ions," *Journal of Colloid and Interface Science*, vol. 606, pp. 510–517, 2022.

[40] Z. J. Xie, X. Y. Bao, and C. F. Peng, "Highly sensitive and selective colorimetric detection of methylmercury based on DNA functionalized gold nanoparticles," *Sensors*, vol. 18, no. 8, p. 2679, 2018.

[41] L. Yan, Z. Chen, Z. Zhang, C. Qu, L. Chen, and D. Shen, "Fluorescent sensing of mercury (II) based on formation of catalytic gold nanoparticles," *The Analyst*, vol. 138, no. 15, pp. 4280–4283, 2013.

[42] Y. Zhao, H. Qiang, and Z. Chen, "Colorimetric determination of Hg (II) based on a visually detectable signal amplification induced by a Cu@ Au-Hg trimetallic amalgam with peroxidase-like activity," *Microchimica Acta*, vol. 184, no. 1, pp. 107–115, 2017.

[43] X. Li, L. Wang, D. Du, L. Ni, J. Pan, and X. Niu, "Emerging applications of nanozymes in environmental analysis: opportunities and trends," *TrAC, Trends in Analytical Chemistry*, vol. 120, Article ID 115653, 2019.

[44] L. Q. Zheng, X. D. Yu, J. J. Xu, and H. Y. Chen, "Re- versible catalysis for the reaction between methyl orange and $NaBH_4$ by silver nanoparticles," *Chemical Communications*, vol. 51, no. 6, pp. 1050–1053, 2015.

[45] N. Logan, C. McVey, C. Elliott, and C. Cao, "Amal- gamated gold-nanoalloys with enhanced catalytic activity for the detection of mercury ions (Hg^{2+}) in seawater samples," *Nano Research*, vol. 13, no. 4, pp. 989–998, 2020.

[46] Z. Mohammadpour, A. Safavi, and M. Shamsipur, "A new label free colorimetric chemosensor for detection of mercury ion with tunable dy- namic range using carbon nanodots as enzyme mimics," *Chemical Engineering Journal*, vol. 255, pp. 1–7, 2014.

[47] G. L. Wang, L. Y. Jin, X. M. Wu, Y. M. Dong, and Z. J. Li, "Label-free colorimetric sensor for mercury (II) and DNA on the basis of mer- cury (II) switched-on the oxidase-mimicking activity of silver nanoclusters," *Analytica Chimica Acta*, vol. 871, pp. 1–8, 2015.

[48] G. L. Wang, X. F. Xu, L. H. Cao, C. H. He, Z. J. Li, and C. Zhang, "Mercury (II)-stimulated oxidase mimetic activity of silver nanoparticles as a sensitive and selective mercury (II) sensor," *RSC Advances*, vol. 4, no. 12, pp. 5867–5872, 2014.

[49] Y. W. Wang, L. Wang, F. An et al., "Graphitic carbon nitride supported platinum nanocomposites for rapid and sensitive colorimetric detection of mercury ions," *Analytica Chimica Acta*, vol. 980, pp. 72–78, 2017.

[50] C. Quintana, M. P. Cifuentes, and M. G. Humphrey, "Transition metal complex/gold nanoparticle hybrid materials," *Chemical Society Reviews*, vol. 49, no. 8, pp. 2316–2341, 2020.

[51] E. Piscopiello, "Leander tapfer, marco vittori antisari, pasquale Pa- iano, paola prete, and nicola lovergine. Formation of

epitaxial gold nanois- lands on (100) silicon," *Physical Review B*, vol. 78, 2008.

[52] J. Spadavecchia, P. Prete, N. Lovergine, L. Tapfer, and R. Rella, "Au nanoparti- cles prepared by physical method on Si and sapphire substrates for biosensor applications," *The Journal of Physical Chemistry B*, vol. 109, no. 37, pp. 17347–17349, 2005.

[53] I. Miccoli, R. Spampinato, F. Marzo, P. Prete, and N. Lovergine, "Dc-magnetron sputtering of ZnO: Al films on (00.1) Al_2O_3 substrates from slip-casting sin- tered ceramic targets," *Applied Surface Science*, vol. 313, pp. 418–423, 2014.

[54] A. I. Cervantes-Macías, C. A. Huerta-Aguilar, and T. Pandiyan, "Carlos A Huerta-Aguilar, and Thangarasu Pandiyan. ZnO-Fe_3O_4-Au hybrid composites for thioanisole ox- idation under visible light: experimental and theoretical studies," *Journal of Cluster Science*, vol. 28, no. 4, pp. 1897–1922, 2017.

[55] H. J. Lee, J. H. Mun, H. Oh et al., "Enhanced photodetec- tor performance in gold nanoparticle decorated ZnO microrods," *Materials Characterization*, vol. 171, Article ID 110813, 2021.

[56] P. Prete, N. Lovergine, and L. Tapfer, "Nanostructure size evolution during Au-catalysed growth by carbo-thermal evaporation of well-aligned ZnO nanowires on (100)Si," *Applied Physics A*, vol. 88, no. 1, pp. 21–26, 2007.

[57] P. Wang, D. Wu, Y. Ao, C. Wang, and J. Hou, "ZnO nanorod arrays co-loaded with Au nanoparticles and reduced graphene oxide: synthe- sis, characterization and photocatalytic application," *Colloids and Surfaces A: Physicochemical and Engineering Aspects*, vol. 492, pp. 71–78, 2016.

[58] M. T. Alula, P. Lemmens, L. Bo, D. Wulferding, J. Yang, and H. Spende, "Peter Lemmens, Liu Bo, Dirk Wulferding, Jyisy Yang, and Hendrik Spende. Preparation of silver nanoparticles coated ZnO/Fe_3O_4 composites using chemical reduction method for sensitive detection of uric acid via surface-enhanced Raman spectroscopy," *Analytica Chimica Acta*, vol. 1073, pp. 62–71, 2019.

[59] L. V. Quang and A. T. Vu, "Preparation of Au/ZnO/Fe_3O_4 composite for degradation of tartrazine under visible light," *Bulletin of Chemical Reaction Engineering and Catalysis*, vol. 18, no. 1, pp. 71–84, 2023.

[60] M. T. Alula and M. L. Madingwane, "Colorimetric quantification of chromium (VI) ions based on oxidoreductase-like activity of Fe_3O_4," *Sensors and Actuators B: Chemical*, vol. 324, Article ID 128726, 2020.

[61] M. T. Alula, P. Lemmens, and M. L. Madingwane, "Peter Lemmens, and Mildred Lesang Madingwane. Determination of cysteine via its inhibition of catalytic activity of silver coated ZnO/Fe_3O_4 composites used for conversion of 4-nitrophenol into 4- aminophenol," *Microchemical Journal*, vol. 156, Article ID 104976, 2020.

[62] P. L. Hariani, M. Faizal, R. Ridwan, M. Marsi, and D. Setiabudidaya, "Muhammad faizal, ridwan ridwan, marsi marsi, and dedi setiabudidaya. Synthesis and properties of Fe_3O_4 nanoparticles by co-precipitation method to removal procion dye," *International Journal of Environment and Sustainable Development*, vol. 4, no. 3, pp. 336–340, 2013.

[63] D. D. S. Biron, V. Santos, and C. P. Bergmann, "Synthesis and characterization of zinc oxide obtained by combining zinc nitrate with sodium hydroxide in polyol medium," *Materials Research*, vol. 23, no. 2, 2020.

[64] M. M. Ba-Abbad, D. Ewis, A. W. Mohammad, Mahmoudi, and A. Benamour, "Abdul Wahab Mo- hammad, and Ebrahim Mahmoudi. Synthesis of Fe_3O_4 nanoparticles with dif- ferent shapes through a co-precipitation method and their application," *Journal of the Minerals Metals & Materials Society*, vol. 74, no. 9, pp. 3531–3539, 2022.

[65] M. Mazhani, M. T. Alula, and D. Murape, "SERS assisted monitoring of catalytic reduction reaction using silver-magnetic nanocompos- ites," *Materials Chemistry and Physics*, vol. 265, Article ID 124487, 2021.

[66] K. Petcharoen and A. J. M. S. Sirivat, "Synthesis and characterization of magnetite nanoparticles via the chemical co-precipitation method," *Materials Science and Engineering: B*, vol. 177, no. 5, pp. 421–427, 2012.

[67] Y. Holade, N. Sahin, K. Servat, T. Napporn, and K. Kokoh, "Recent advances in carbon supported metal nanopar- ticles preparation for oxygen reduction reaction in low temperature fuel cells," *Catalysts*, vol. 5, no. 1, pp. 310–348, 2015.

[68] S. E. Skrabalak, B. J. Wiley, Y Xia, M. Kim, and E. V. Formo, "On the polyol synthesis of silver nanostructures: glycolaldehyde as a reducing agent," *Nano Letters*, vol. 8, no. 7, pp. 2077–2081, 2008.

[69] A. A. B. Christus, A. Ravikumar, P. Panneerselvam, and K. Radhakrishnan, "ishnan. A novel Hg (II) sensor based on Fe_3O_4@ZnO nanocomposite as per- oxidase mimics," *Applied Surface Science*, vol. 449, pp. 669–676, 2018.

[70] P. Miao, Y. Tang, and L. Wang, "DNA modified Fe_3O_4@Au magnetic nanoparticles as selective probes for simultaneous detection of heavy metal ions," *ACS Applied Materials & Interfaces*, vol. 9, no. 4, pp. 3940–3947, 2017.

[71] K. Feke, M. T. Alula, H. Spende, A. Waag, and P. Lemmens, "Synthesis of a recoverable CuS/Fe_3O_4 composite structure with enhanced oxidase-like activity for detection of chromium (VI)," *Journal of Cluster Science*, vol. 34, no. 2, pp. 1009–1018, 2022.

[72] A. F. M. Santos, L. J. A. Macedo, M. H. Chaves et al., "Hybrid self-assembled materials constituted by ferromagnetic nanoparticles and tannic acid: a theoretical and experimental investigation," *Journal of the Brazilian Chemical Society*, vol. 27, pp. 727–734, 2015.

[73] B. Manikandan, T. Endo, S. Kaneko, K. R. Murali, and R. John, "Properties of sol gel synthesized ZnO nanoparticles," *Journal of Materials Science: Materials in Electronics*, vol. 29, no. 11, pp. 9474–9485, 2018.

[74] A. K. Zak, R. Razali, W. H. A. Majid, and M. Darroudi, "Synthesis and characterization of a narrow size distribution of zinc oxide nanopar- ticles," *International Journal of Nanomedicine*, vol. 6, pp. 1399–1403, 2011.

[75] L. Abraham, "Light scattering and plasmonic response of Au-Fe_3O_4 nanoparticles," *SN Applied Sciences*, vol. 2, no. 11, pp. 1–8, 2020.

[76] G. Geng, P. Chen, B. Guan et al., "Sheetlike gold nanostructures/graphene oxide composites via a one-pot green fabrication protocol and their interesting two-stage catalytic behaviors," *RSC Advances*, vol. 7, no. 82, pp. 51838–51846, 2017.

[77] T. L. Néel, M. Bayle, and P. Bertoncini, "Functionalized gold nanoparticles and nanoplatelets synthesized using plant extract and their potential for surface-enhanced Raman spectroscopy," *Nano-Structures & Nano-Objects*, vol. 30, Article ID 100855, 2022.

[78] F. M. M. Aldosari, "Characterization of labeled gold nanoparticles for surface-enhanced Raman scattering," *Molecules*, vol. 27, no. 3, p. 892, 2022.

[79] S. Tang, H. Liu, M. Wang et al., "Further enhancement of SERS signals from Au@Ag@PSPAA core–shell nanoparticles surrounded by Ag nanoplatesAu@Ag@PSPAA core–shell

nanoparticles surrounded by Ag nanoplates," *Materials Chemistry and Physics*, vol. 225, pp. 60–63, 2019.

[80] G. Q. Wallace, M. Tabatabaei, and F. Lagugné-Labarthet, "Towards attomolar detection using a surface-enhanced Raman spectroscopy platform fabricated by nanosphere lithography," *Canadian Journal of Chemistry*, vol. 92, no. 1, pp. 1–8, 2014.

[81] Y. Zhang, Y. Hu, G. Li, and R. Zhang, "A composite pre- pared from gold nanoparticles and a metal organic framework (type MOF-74) for determination of 4-nitrothiophenol by surface-enhanced Raman spec- troscopy," *Microchimica Acta*, vol. 186, pp. 1–10, 2019.

[82] L. Bai and J. Mei, "Low amount of Au nanoparticles deposited ZnO nanorods heterojunction photocatalysts for efficient degradation of p- nitrophenol," *Journal of Sol-Gel Science and Technology*, vol. 94, no. 2, pp. 468–476, 2020.

[83] Y. J. Long, Y. F. Li, Y. Liu, J. J. Zheng, J. Tang, and C. Z. Huang, "Visual observation of the mercury-stimulated peroxidase mimetic activity of gold nanoparticles," *Chemical Communications*, vol. 47, no. 43, pp. 11939–11941, 2011.

[84] Y. Chen, Y. Zhang, Q. Kou et al., "Enhanced catalytic reduction of 4-nitrophenol driven by Fe_3O_4-Au magnetic nanocom- posite interface engineering: from facile preparation to recyclable application," *Nanomaterials*, vol. 8, no. 5, p. 353, 2018.

[85] X. Zhao, Z. Li, Y. Deng, Z. Zhao, X. Li, and Y. Xia, "Facile synthesis of gold nanoparticles with alginate and its catalytic activity for reduction of 4-nitrophenol and H_2O_2 detection," *Materials*, vol. 10, no. 5, p. 557, 2017.

[86] Y. He and L. Zheng, "Gold nanoparticle-catalyzed clock reaction of methy- lene blue and hydrazine for visual chronometric detection of glutathione and cysteine," *ACS Sustainable Chemistry & Engineering*, vol. 5, no. 10, pp. 9355–9359, 2017.